Drag Reduction for Trucks by Active Flow Control of the Wake Behind the Trailer Using Large-Eddy Simulation

Mohammad El-Alti*, Per Kjellgren and Lars Davidson

Division of Fluid Dynamics,
Department of Applied Mechanics
Chalmers University of Technology,
SE-412 96 Göteborg, Sweden

A condensed form of this paper will be presented at the 6th International Symposium on Turbulence, Heat and Mass Transfer, September 14-18, Rome, Italy

Abstract

Several hundred of large-eddy simulations with active flow control have been carried out proposing a novel rear-end of a trailer. It is found that for certain configurations, a reduction of aerodynamic drag by up to 30% or more is achieved. The reduction is mainly due to a pressure recovery on the flap surface and the rear-end of the trailer. The variables of AFC are investigated and optimized using response surface methodology. A thorough analysis of the mechanism of flow control and the flow characteristics of the forced and unforced case are discussed. The slot location, span-wise mesh and domain size, periodic blowing and suction versus periodic blowing and turbulence modeling investigations are carried out in order to evaluate the achieved drag reduction.

*Author to whom all correspondence should be addressed; electronic mail: mohammad.el-alti@chalmers.se

Contents

1 Introduction

1.1 Background

The aerodynamics of today's trucks is far from optimal. While vehicle manufacturers of personal cars develop their sophisticated models that are designed for low fuel consumption so is the rear end of all trucks in principle squared with four perpendicular corners. Truck manufacturers around the world have begun to realize the great need that exists to reduce fuel consumption and improve environmental performance of trucks. In order to develop more environmentally friendly vehicles to meet the growing environmental requirements, the harder international competition within the heavy-vehicle industry and the still increasing fuel prices, one has to include and consider the trailer in the aerodynamic design development [1] and implement advanced active flow control techniques.

Most of the drag on a truck is caused by the wake behind the trailer which is called the base drag. It is introduced due to the sharp edges on the rear-end where the flow naturally separates. This effect gives rise to a large low-pressure region and thus increases the pressure difference between the front and back. The large low-pressure region acts as a force that sucks the whole truck backwards. An effective way to increase the pressure on the back is by introducing angled flaps. By introducing the flaps at an angle less than the natural separation angle, the wake becomes narrower which decreases the base drag. If the angle is increased, the base drag increases again. The idea is now to further decrease the base drag by attaching the flow onto the flap surface again. The attachment process is done using active flow control (AFC). The idea of using flaps and reattaching the separated flow is in line with research with successful results on tilt-rotor aircrafts done by the authors in [2, 3] that was a continuation from previous research [4, 5, 6].

Two main flow physical goals are expected from this technique. The first one is to narrow the size of the wake by attaching the separated flow and the second is to make the wake less intensive. The former one is achieved by the introduction of flaps at high angle at the rear-end and reattaching the naturally separated flow onto the flap surface. The reattachment process is done by the increased level of turbulence close to the separation point that re-energizes the weak boundary layer, that is to separate. The latter one is achieved by the creation of small vortices, that are generated by the blowing and suction of the AFC, and whose intensity increases downstream. These vortices develop a shear layer that destroys the dissipative wake structure and makes the wake less intensive.

1.2 Flow control

Flow control is probably the hottest research area in fluid mechanics. To be able to manipulate a flow field in order to achieve desired engineering beneficial results seems to be the way to meet today's demands in competitive and efficient solutions for the automotive industry.

> "The process or operation by which certain characteristics of a given flow are manipulated in such a way as to achieve improvements of a specific technical performance."(Fiedler [7]).

This definition gives a good description of the field of flow control. Today, the demands in environmental friendly, economical and efficient vehicles are one of the driving forces for the developments in this hot field. The birth of this field scientifically goes back to 1904 when Prandtl presented his work "On Fluid Motion with Very Small Friction" at the Third International Congress of Mathematicians held at Heidelberg, Germany. The boundary-layer theory was introduced and controlled actively by suction in order to delay separation on a surface of a cylinder. The advancement in this field was rapid during the Second World War and the cold war. The needs of efficient, competitive and fast aircrafts, missiles and other military equipment which includes fluid dynamics were not targeted without the use of flow control strategies. Some of the advancements include delaying transition in laminar flows to achieve drag reduction. Civilian interest of flow control grew in connection with the energy crises 1973 where the goal was to conserve energy by e.g. reducing drag for civilian air, sea and land vehicles. By the use of computational fluid dynamics more applications of flow control has been investigated toward optimal design targets. This includes reactive control strategies and the developments of micro electromechanical systems (MEMS) [8].

There are different views of how to classify flow control strategies [8]. The most common one is by considering the energy input into the system, as shown in Figure 1(a). If no energy is used while controlling the flow, the flow control is passive and by the use of energy the flow control becomes active.

1.2.1 Passive and Active Flow Control

Passive flow control is achieved by geometrical modifications or additional geometrical configurations in order to control the flow or to generate a desired behaviour. Vortex generator is a typical example of passive flow control where a small vane creates a vortex. It is used on airplanes to delay separation at the cost of increasing the drag. The introduction of flaps in this work is a kind of passive flow control, the idea is to narrow the size of the wake by maintaining the flow reattached on the flap surface.

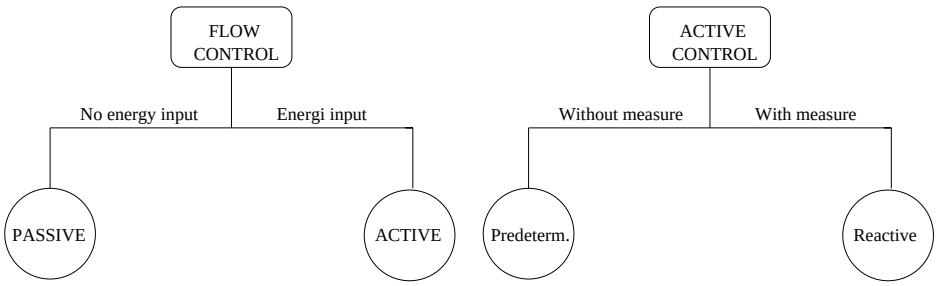

(a) Classification of flow control. (b) Classification of active flow control.

Figure 1: Classification diagram of flow control methods.

Active flow control is further classified in predetermined and reactive control. The predetermined case is also called an open-loop active flow control. Here predetermined energy is used as input without measuring any quantity in the flow field. A typical device is an actuator with a mechanical motion in order to control the flow. The effect is linear or periodic excitation of flow in desired regions. Figure 1(b) shows this classification. Reactive flow control is when the state of a variable is measured and used in the control process. Reactive flow control can be divided into two cases depending on which variable is measured. If the measured variable is also the controlled one, the reactive control is a closed feedback loop control, otherwise it is an open feed-forward one.

In this work, predetermined active flow control is used. This choice is based on several basic principles. It is much easier to start an investigation by predetermined control. If there is no potential net effect, then feedback control can be the next step. If there is an effect, feedback control can be the next step to further improve the flow control. We also assume that in general the trucks are driven at constant velocity magnitude at highways, in Sweden around 90 km/h. Thus there is less need to have feedback control if the truck velocity is constant. However the weather (e.g. side-winds) will probably affect the desired control but such considerations is out of the scope of this work yet. Future work will probably include such investigations.

The engineering end-results e.g. drag reduction or reducing noise levels, is a consequence of the strategies in controlling the flow. Flow control is used to delay or advance transition, prevent or provoke separation and suppress or enhance turbulence. In this work, flow control is used to enhance turbulence on the flap surface which in turn delays the separation and finally reduce the size of the wake and the level of turbulence in the wake. It is not always obvious which strategy to use in order to control the flow. There are always bi-effects which one has to deal with to get the desired result. The actuators

will e.g. increase the level of noise that could be disturbing for passenger cars behind the truck; the truck driver will probably not hear the increased level of noise regarding that the length of the truck is over 13 m.

1.2.2 Other efforts

Several efforts have been carried out in order to minimize the base drag on trucks. Both pure passive and combined with active flow control strategies. The investigations in [9] and [10] both used passive devises mounted at the rear-end of the trailer. In [9] a drag reduction of 15% was reached by using base flaps inclined at 15°. In [10] they tried with vortex generators, base flaps and boattail. The vortex generators actually increased the drag but the flaps and boattail showed marginal drag reduction.

Several active flow control efforts have been carried out, both with and without flap. Without flap was investigated in [11] and [12], the authors in [11] used a circular cylinder that had a build-in actuator and reached drag reduction of 20%. In [12] they used closed-loop control on a blunt trailing edge and reached 10% drag reduction. In [13] and [14] they used base flaps with AFC and reached drag reduction below 10%. One successful effort was done in [15] that achieved drag reduction of about 30% using steady blowing. This is promising result but the use of steady blowing is energy consuming and the net drag reduction is not that high.

Having these efforts in mind leads us to do a thorough parameter study with optimization and use periodic blowing that is much more effective than steady blowing with almost the same end results [16].

1.3 Optimization

The surrogate models are adopted as optimization approach. The specific model is the polynomial response surface methodology (RSM). The main advantage of this method is that all candidate design can be run parallel in time. The model does not require information between the candidates during the optimization. This is very useful when running experiments or heavy CFD computations. The choice of this optimization strategy is mainly because it is robust and that the aim is to find a region of feasible design instead of using the usual gradient-based local minimum/maximum seeking optimization strategies. It is the understanding of the response on each parameter on the system that makes this algorithm useful during physical fluid analysis.

The idea of RSM is to build an empirical model of the true response surface of the system. The true response surface is governed by physical laws. The obtained data from the design candidates are used to build a mathematical best fitting model. A second-order polynomial model has been adopted in order to capture the nonlinearity. The model also includes

interaction terms of the different parameters.

We follow the procedure in [17]. If the true response is denoted as y, the design parameters $x_1, x_2, x_3, ..., x_n$, then we have the following statement

$$y = f(x_1, x_2, x_3, ..., x_n) + \epsilon \tag{1}$$

where ϵ is all sources of errors. By using second-order RSM the regression model is written as

$$y = \beta_0 + \sum_{i=1}^{k} \beta_i x_i + \sum_{i=1}^{k} \beta_{ii} x_i^2 + \sum_{i<j} \sum_{j=2}^{k} \beta_{ij} x_i x_j + \epsilon \tag{2}$$

where β's are the regression coefficients, x_i is the i^{th} design parameter and k is the total number of design parameters. By minimizing the error using least-square fit of the regression coefficients the approximation of the true response $\hat{y}$ is

$$\hat{y} = b_0 + \sum_{i=1}^{k} b_i x_i + \sum_{i=1}^{k} b_{ii} x_i^2 + \sum_{i<j} \sum_{j=2}^{k} b_{ij} x_i x_j \tag{3}$$

The b's are now the least-square estimators of the regression coefficients.

In order to check the quality of the estimated regression model, some statistical coefficients are calculated. The coefficient of multiple determination (R^2) and the adjusted one (R^2_{adj}) defined in equation 4 and 5 are a measures of how much the variability of y is reduced using the regressor variables $x_1, x_2, x_3, ..., x_k$. $R^2_{adj} = 1$ corresponds to perfect fit. The difference between R^2 and R^2_{adj} is that if a regressor is added to the model, R^2 will increase despite that the added regressor will not improve the model; however the R^2_{adj} will decrease. In order to increase the model fit and thus increase R^2 and R^2_{adj}, it is possible to check the individual regressors using test statistic and reject the ones that does not fulfil a prescribed criterion. Due to lack of time these tests have not been carried out. R^2 and R^2_{adj} are defined as

$$R^2 = 1 - \frac{SS_E}{SS_T} \tag{4}$$

$$R^2_{adj} = \frac{1 - SS_E/(n-p)}{SS_T/(n-1)} \tag{5}$$

$SS_E = \sum_{i=1}^{n} (y_i - \hat{y}_i)^2$ is the sum of square of errors, $SS_T = \sum_{i=1}^{n} (y_i - \bar{y}_i)^2$ is the total sum of square, n is the number of observations and p is the number of regressors.

In order to check outliers, the residuals and the studentized residuals (r_i) are analyzed. The studentized residuals are obtained by scaling the residuals

in such a way to obtain constant variance of each residual $Var(r_i) = 1$. Outliers have been removed if $|r_i| > 3$.

It is important to choose appropriate values of the parameters for each design candidate, The method of the statistical appropriate choice for best fit is called "Design of Experiment" (DOE). There are a lot of DOE methods for second-order models and to decide which one to choose is problem dependent. There are e.g. central composite design (CCD), spherical CCD, Box Behnken design and face-centered central composite design. Each design has specific advantage/disadvantage considering the problem at hand. The chosen design is the inscribed central composite design shown in figure 2. It has the rotability property and does not use any design candidate outside the prescribed design space, thus it is good on the central subset of the design space [18]. The rotability property ensure that if two design candidates have the same distance from the origin, then the predicted values have equal predicted variance $NVar[\hat{y}(x)]/\sigma^2$. It is good to have two design spaces, one overall and one close to extreme locations. Due to lack of time, only one design space was investigated.

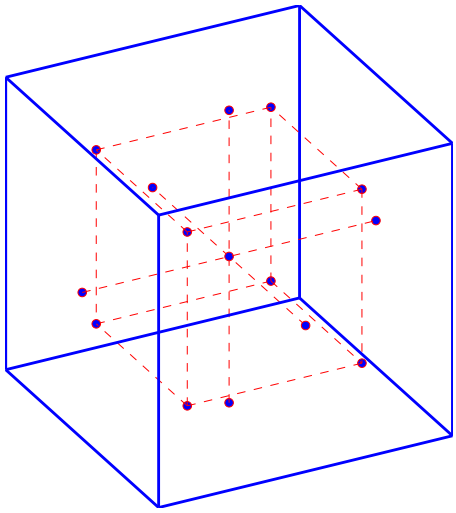

Figure 2: Inscribed central composite design, DOE for RSM, blue line is the boundary of the design space.

2 Numerical Method

2.1 Large-eddy simulation

The flow behind the truck is unsteady and the pulsating (i.e. oscillating) jets are used as forcing. Thus the modeling strategy must be transient. The modeled actuator is very narrow and the excitation velocity is about 50%

of the free stream velocity. The actuation frequency is also much higher than the Strouhal frequency. Thus fine resolution both in space and time is needed. Therefore in order to make accurate prediction of the turbulent flow, large-eddy simulation is used. It provides both instantaneous field data and high accuracy. The Reynolds number is $200,000$ which is in the range of manageable LES. Higher Reynolds number like full-scale flow would have enforced us to use a hybrid LES/RANS approach, such as DES. However a comparison of several turbulence models is carried out in section 3.5.4. The commercial FlowPhys ver. 2.0 software is used for the computations in this work. It has a semi-implicit, fractional step finite element solver.

The filtered Navier-Stokes equations read

$$\frac{\partial \bar{u}_i}{\partial t} + \frac{\partial}{\partial x_j}\left(\bar{u}_i \bar{u}_j\right) = -\frac{1}{\rho}\frac{\partial \bar{p}}{\partial x_i} + \nu \frac{\partial^2 \bar{u}_i}{\partial x_j \partial x_j} - \frac{\partial \tau_{ij}}{\partial x_j} \tag{6}$$

where $\tau_{ij} = \overline{u_i u_j} - \bar{u}_i \bar{u}_i$ is the sub-grid scale stresses modeled as

$$\tau_{ij} - 1/3\delta_{ij}\tau_{kk} = -2\nu_{sgs}\bar{s}_{ij} \tag{7}$$

where ν_{sgs} is

$$\nu_{sgs} = \left(C_S f \Delta\right)^2 \sqrt{2\bar{s}_{ij}\bar{s}_{ij}} \tag{8}$$

and $\bar{s}_{ij}$ is

$$\bar{s}_{ij} = 1/2\left(\frac{\partial \bar{u}_j}{\partial x_j} + \frac{\partial \bar{u}_j}{\partial x_i}\right) \tag{9}$$

The Smagorinsky model (7) for the sub-grid scales is used with the Smagorinsky constant $C_S = 0.20$. In the near-wall region ($20\ cm$) the filter width is reduced using Van Driest damping function.

$$f = 1 - e^{-y^+/A^+} \tag{10}$$

where $A^+ = 25$ and y^+ is calculated by searching the closest distance between a node in the domain and the wall node.

The temporal discretization is the explicit four-step Runge-Kutta scheme for the convection terms and the Crank-Nicholson method for the diffusion terms. The spatial discretization scheme is the pure central difference (CD).

The time-step size was controlled by an adaptive time stepper that kept the max Courant number equal to two. The check was done every 10th time-step. The number of time-steps was typically between $100\,000 - 200\,000$ and the time-step size varied between 10^{-4} and $6 \cdot 10^{-5}$.

The forcing is modeled as a transient velocity inlet and the governing variables are the slot width, the velocity (both magnitude and direction) and the frequency. The RMS momentum from the slot is defined as

$$J_{rms} = \int \rho u_{rms}^2 \, dh = \rho u_{rms}^2 \Delta h \tag{11}$$

Δh is the effective slot width. Further we define the momentum-coefficient as

$$C_{\mu\ rms} = \frac{J_{rms}}{w\frac{1}{2}\rho u_\infty^2} = \frac{u_{rms}^2 \Delta h}{w\frac{1}{2}u_\infty^2} \tag{12}$$

where w is the width of the truck, from 12 the velocity in the slot is given by

$$u_{rms} = \sqrt{\frac{C_{\mu\ rms}\ w\ u_\infty^2}{2\Delta h}} \tag{13}$$

We further assume that the forcing is pure sinusoidal i.e.

$$u(t) = \sqrt{2} u_{rms} \sin(2\pi F t) \tag{14}$$

Finally we define the non-dimensional forcing frequency as

$$F^+ = \frac{F \cdot X_{TE}}{U_\infty} \tag{15}$$

where X_{TE} is the distance from the slot to the trailing edge of the flap.

2.2 Computational domain

We use a simplified truck model in our simulations. The truck is simplified as a rectangular bluff body with typical width ($w = 2.6\ m$) and length ($l = 13.0\ m$) relevant for a real truck and assuming periodicity in the third direction (height), i.e. the domain is three-dimensional (figure 3 and 5). The size of the slice is also investigated in order to have a consistent computational configuration (section 3.5.1). The truck is mounted with angled flaps on the rear-end in which the oscillating synthetic jet actuators are placed (fig. 3). The actuators are modeled as a time-varying boundary condition (slot). The slot extends over the entire height (z) of the truck.

The truck geometry is shown in figure 3 and 4. The inlet flow is modeled as inlet boundary condition (BC) with prescribed constant free-stream velocity, $U_\infty = 25\ m/s$. The Reynolds number is reduced to 200 000 by increasing the viscosity to $\mu = 3.25 \cdot 10^{-4}$. The outlet BC is the standard outlet with zero-gradient. The side-walls are prescribed frictionless walls, i.e. slip BC.

The computational mesh is shown in figures 5, 6 and 7. The number of nodes in the wake and the flap region is very large compared to those in the free-stream region. The mesh size is around $1.4 - 3.3$ million nodes and consist of unstructured quad elements in the $x - y$ plane and structured quad elements in the span-wise direction. The quality of the mesh was very high close to the wall and in the flap region. At the end of the truck side-walls (prior to the flap) max $y^+ < 2$, mean $y^+ \sim 1$, max $\Delta x^+ < 30$, mean $\Delta x^+ \sim 20$, and Δz^+ for the different cases are given in section 3.5.1.

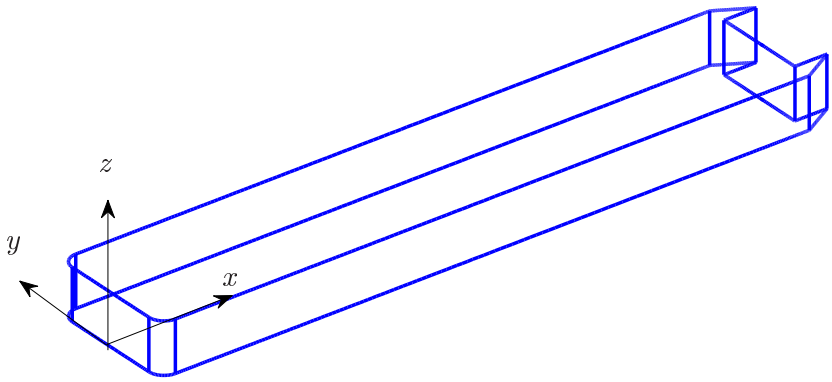

Figure 3: Simplified truck model. Inlet at $x = -12w$; outlet at $x = 30w$; slip sidewalls at $y = -8.5w$ and $y = 8.5w$.

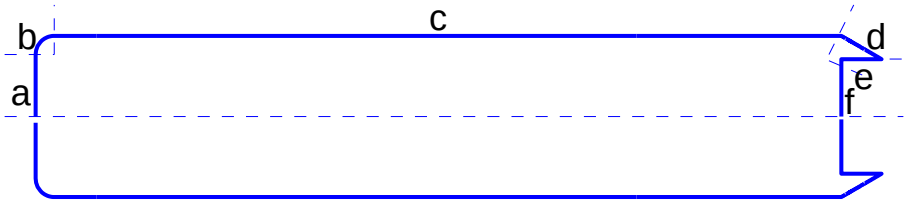

Figure 4: Line representation of the truck showing different parts used in the C_P analysis.

2.3 Procedure and investigated parameters

Several parameters have to be considered in the development process. As a first step an investigation is done by carrying out a large number of computations and varying the geometry of the added flap and governing variables of AFC. In addition to determining flap angle (FA) and length (FL), the slot width, position, velocity amplitude, angle (SA) and frequency have to be determined. We assumed the flap length to be fixed and investigated three flap angle configurations. Assuming also that the slot width and position being fixed and well resolved in each configuration, several velocity amplitudes, angles and frequencies of the slot are varied in order to achieve the largest drag reduction. As a second step, optimization of these parameters is done in order to maximize the drag reduction.

Once the optimal configuration is found, VOLVO 3P and SKAB will in

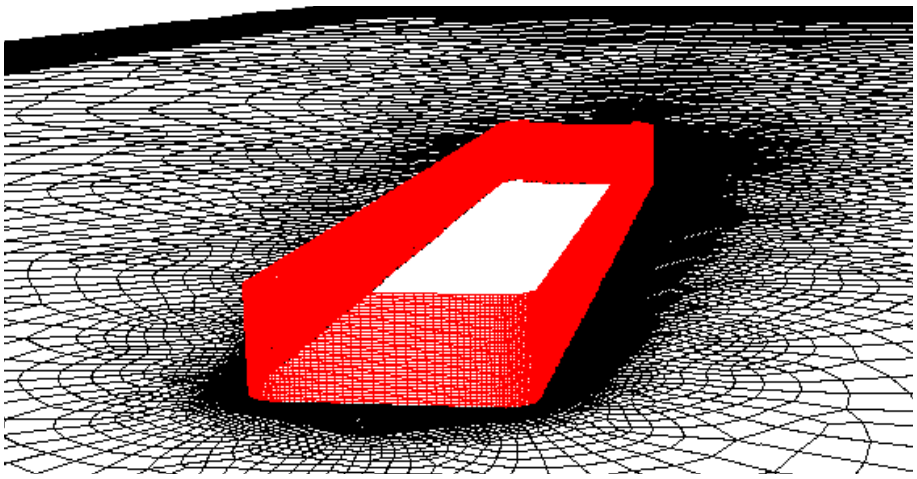

Figure 5: 3D mesh of the computational domain.

Figure 6: Truck side mesh.

the near future manufacture a prototype configuration and make a full-scale test of a truck with the optimal AFC configuration. The actuator that will be used is a simple synthetic-jet actuator capable to produce $C_\mu = 1.0\%$ [19].

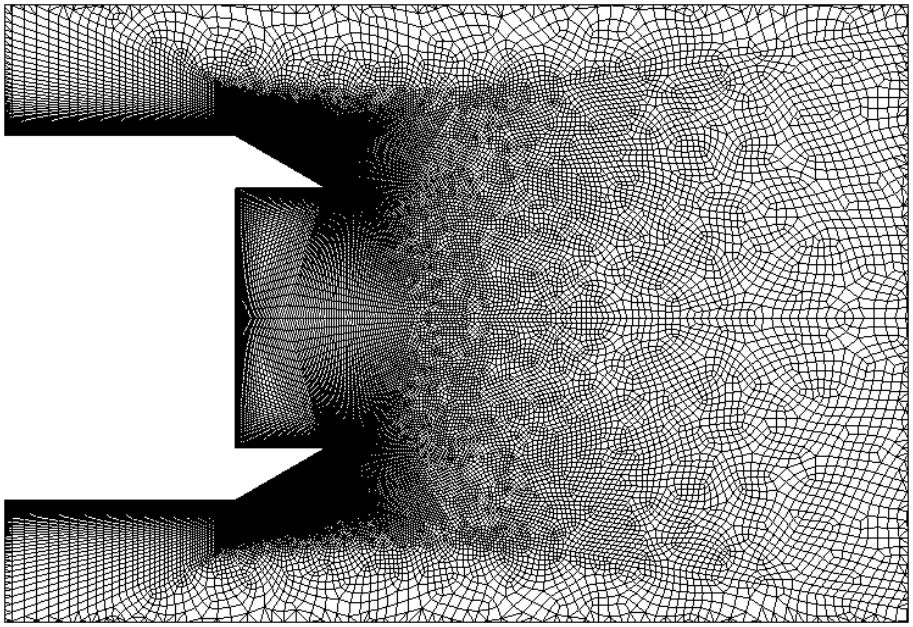

(a) Mesh around the Wake

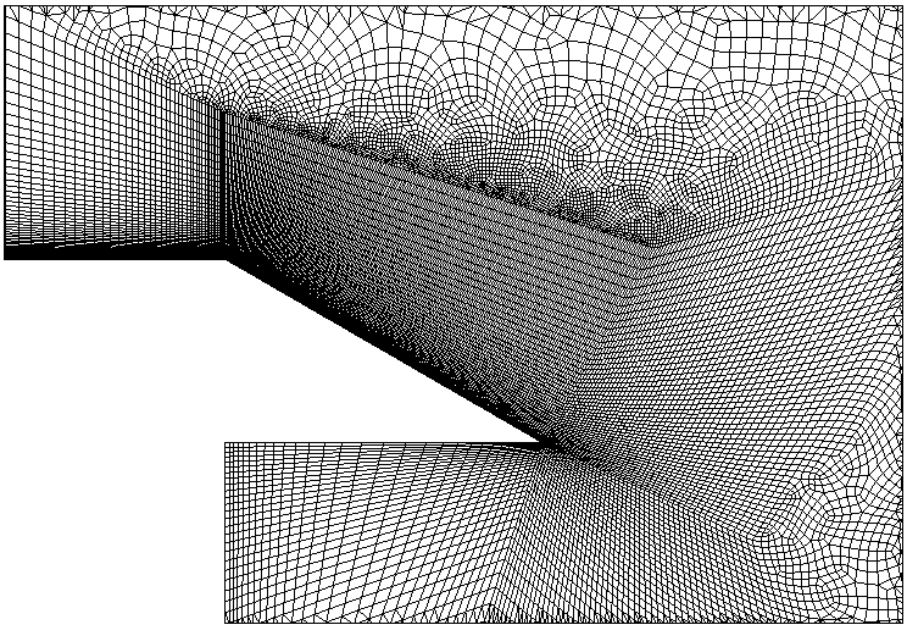

(b) Mesh around the flap

Figure 7: 2D slice of the proposed novel rear-end of trailer, geometry and mesh.

3 Results

The following results are a comparison of the unforced and the forced case. The unforced one is denoted as "AFC OFF" and the forced one as "AFC ON". The specific forced case chosen is one that has shown maximal drag reduction compared with the unforced one. As mentioned in section 1.3 several hundreds of cases were prepared, run and finally optimized. The case that showed low mean drag and reasonable RMS of drag was chosen. The specifications of the chosen case are listed in table 1. The slot width is set to $\Delta h = 5\ cm$ which means that $C_\mu = 1.0\%$ corresponds to $u_{rms} \sim 13.0\ m/s$, see eq. 13 . The location of the slot is at the upper edge of the flap. The span-wise domain size is $0.4\ m$ with 16 cell layers which corresponds to max $\Delta z^+ = 130$ and mean $\Delta z^+ = 100$. Both the instantaneous and time averaged quantities are plotted at three regions of interest: A general plot of the whole truck with upstream and downstream regions, wake region plot and finally flap region plot. FL, FA, and SA denote flap length, flap angle and slot angle respectively. SA is defined relative to the flap surface.

AFC parameter	Value
FL	$0.75\ m$
FA	$30\ deg$
SA	$15\ deg$
C_μ	1.0 %
F^+	0.3

Table 1: Specifications of the forced case

3.1 Instantaneous flow

The instantaneous characteristics of the flow are of high importance to investigate in active flow control. We have chosen to study the instantaneous pressure, velocity and streamlines at a specific instant with locally interesting flow features. We expect that the flow for the unforced case is separated from the flap surface because the flap angle is high enough. Furthermore the separation will develop a strong vortex shedding behind the rear-end of the truck. Instantaneously, each developed vortex will show up as a forward moving low pressure region as shown in figure 8(a). We also notice the strong high pressure at the front region of the truck and the separated flow at the curvature at the intersection of the front and the sides of the truck that is evident in both figures 8(a) and 8(b).

In figure 8(a) we can also see that the pressure on the upper flap is low due to the reversed flow in the separation bubble. The wake region is zoomed in figure 9. It is clear that the low pressure region downstream the flap is suppressed in the forced case (figure 9(b)). We also notice that a smaller

low-pressure region is created at the slot location at which the actuation takes place. We also notice that small vortices are created by the actuation which can be seen at the lower flap in figure 9(b). These small vortices have also been noticed by [6] who did an experiment on flow separation and reattachment by AFC on a flap, deflected at angles larger than the natural separation angle. The Reynolds number was $Re = 1.65 \cdot 10^5$ which is of same order as in the present work. The separation from the flap surface is also shown in both figures 10 and 11 where the instantaneous velocity contours are plotted. For the forced case it can be seen that the wake has been smaller and the vortex-shedding weaker. The instantaneous flow is reattached on the flap surface for the forced case (figure 11(b)).

This conclusion is also confirmed by figure 12 and 13 where the instantaneous streamlines are plotted. The flow is reattached and the small vortices created by the actuation can be seen at the downstream edge of upper flap in figure 13(b). Now the location has been moved further downstream the flap surface. We conclude that these vortices, created by the actuation, are moving downstream the flap surface and create a shear layer in the wake region that makes the vortex-shedding weaker and prevents the interaction between the naturally created shear-layers formed at the upper and lower edges. These vortices are furthermore moving downstream in the wake region with successively increasing size as shown in figure 12(b), destroying the low-pressure dominant wake structure and yielding pressure recovery. The actuation, by its blowing and suction, is re-energizing the boundary layer that is to separate, and interacts with the ambient flow to introduce vortices that rolls down the flap surface. When the flow remains reattached on the flap surface, the wake size is narrowed.

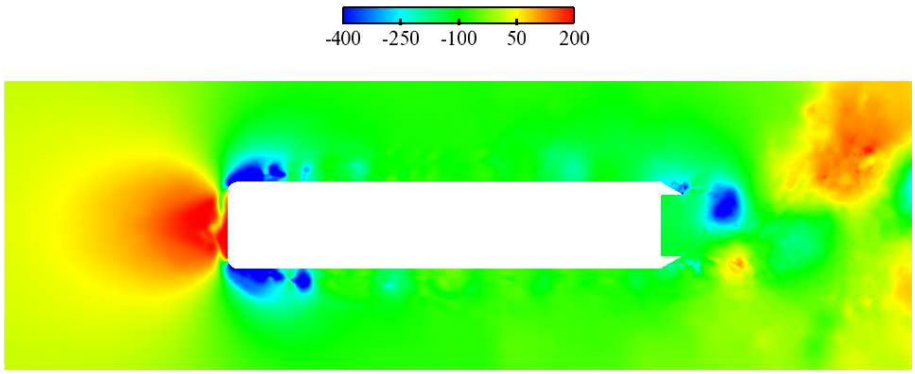

(a) AFC OFF

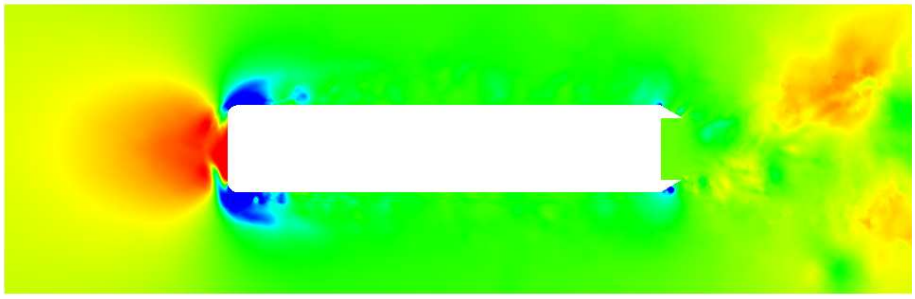

(b) AFC ON

Figure 8: Instantaneous pressure contours. Note the large low-pressure region downstream the upper flap in (a) and how it is suppressed by AFC in (b).

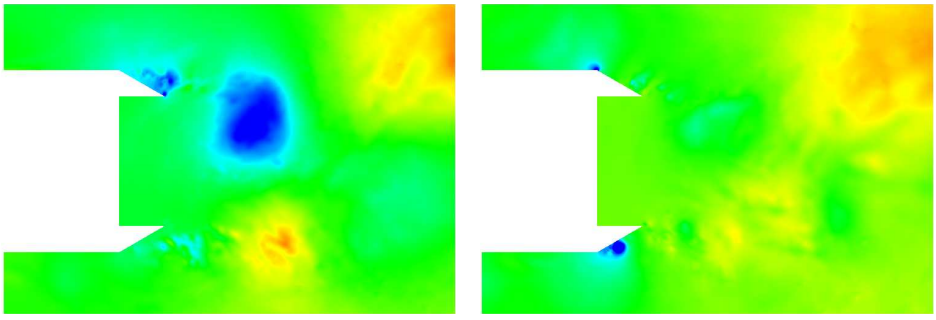

(a) AFC OFF (b) AFC ON

Figure 9: Instantaneous pressure contours, zoom of the wake.

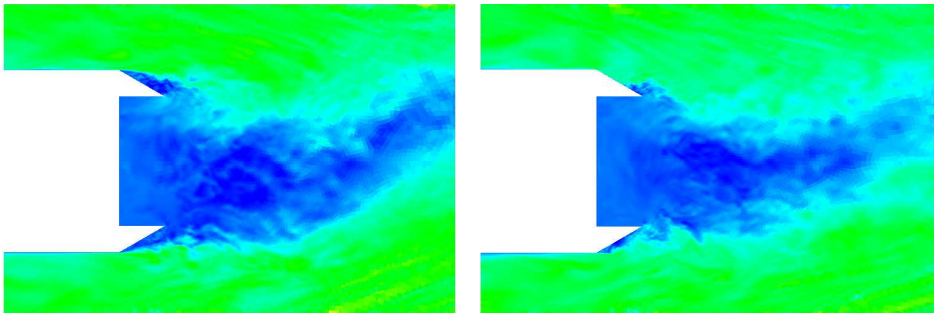

(a) AFC OFF (b) AFC ON

Figure 10: Instantaneous u-velocity contours, zoom around wake region.

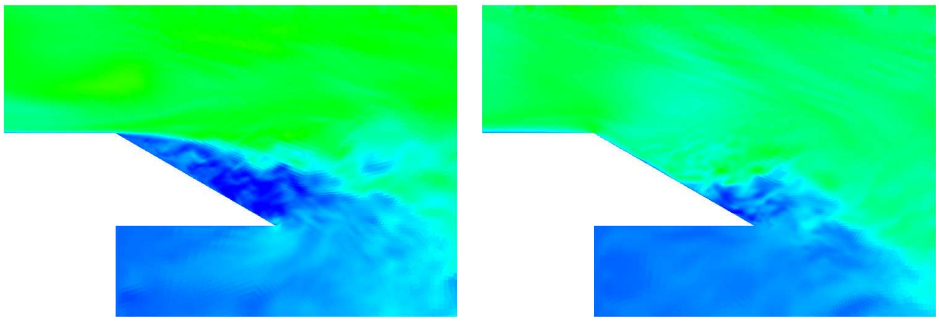

(a) AFC OFF (b) AFC ON

Figure 11: Instantaneous u-velocity contours, zoom around flap region.

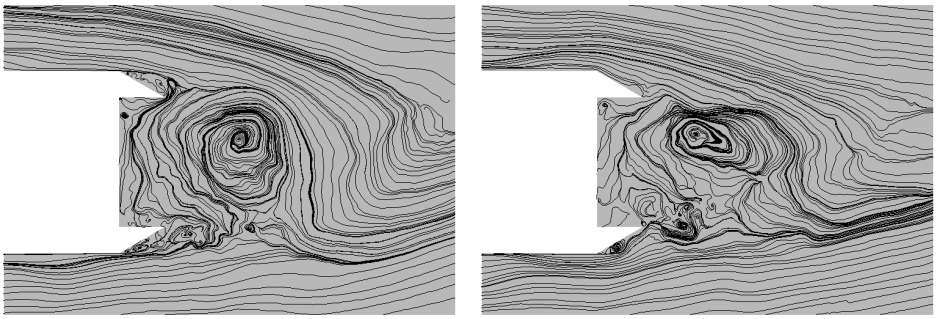

(a) AFC OFF (b) AFC ON

Figure 12: Instantaneous streamlines, zoom around wake region.

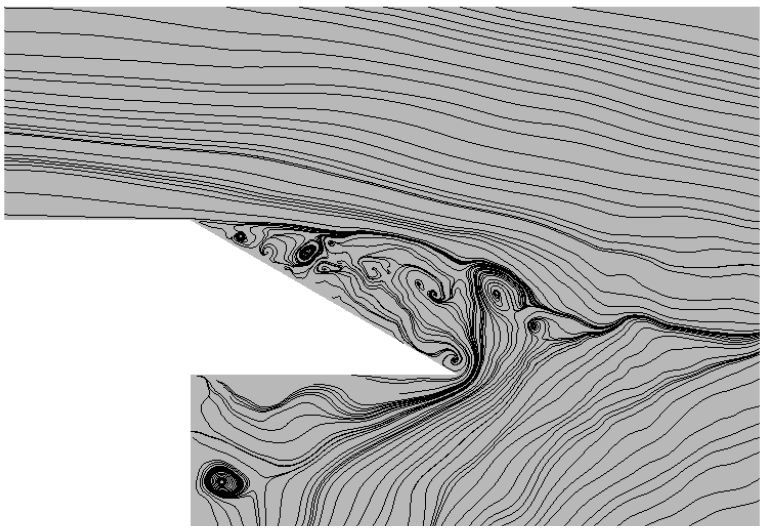

(a) AFC OFF

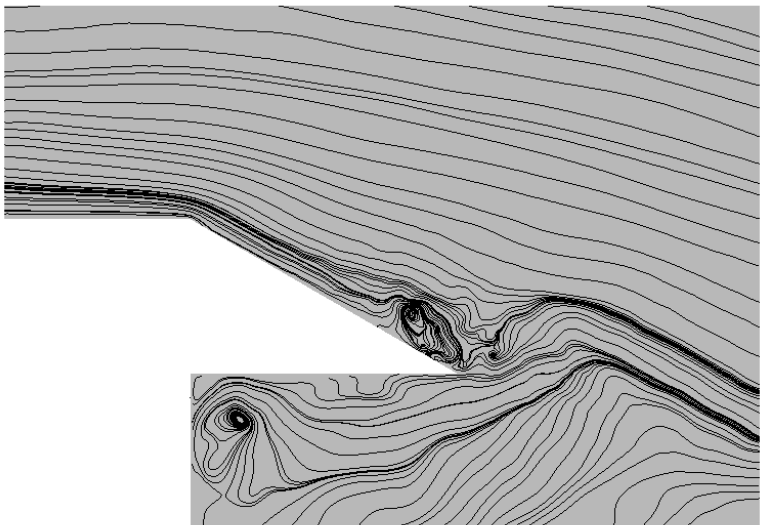

(b) AFC ON

Figure 13: Instantaneous streamlines, zoom around flap region.

3.2 Time-averaged flow and wake structure

The effect of the actuation is further studied by time-averaged flow quantities. Pressure, U-velocity, streamlines and vorticity are investigated. Furthermore in order to study the level of activity in the wake, i.e. the strength of the vortex-shedding, the RMS of pressure is plotted for different regions.

In figure 14 the time-averaged pressure is plotted. With AFC off, we notice the expected large low-pressure region behind the truck caused by the strong vortex-shedding. A low pressure region is also found at the front curvature denoted as b in figure 4. The low-pressure region behind the truck is almost totally suppressed by AFC in figure 14(b). The wake region is zoomed in figure 15. Here we also notice, for the unforced case, the low pressure region on the flap. This region is however advanced upstream in the forced case. We conclude that by AFC a low pressure region is created at the slot location that sucks the flow onto the flap surface.

In figure 16 the time-averaged streamlines are plotted. It is clear that the wake structure is affected in the forced case. The wake region is further zoomed in figures 17 and 18. We notice the smaller wake structure of the forced case both in figures 17(b) and 18(b). The wake is narrowed and has shorter distribution in the free-stream direction.

In figures 19 and 20 the flap region is featured. It is clear that the time-averaged flow is entirely reattached by active flow control. Furthermore the flow coming from the back-side of the truck, up to the flap surface, as reversed flow is prevented by the reattached streamlines. This is one of the reasons why the interaction of the lower and upper shear-layers is prevented.

The time-averaged vorticity is investigated in figure 21 and 22. The latter one is plotted with mean velocity vectors. It is clear that the flow on the upper symmetric half of the truck produces negative vorticity and on the lower half, positive vorticity as shown in figure 21. From figure 22 we can draw several conclusions: first we recognize the separation region in the unforced case, showing both positive and negative vorticity, we also notice the strong positive vorticity evolving from the end of the flap. The forced case in figure 22(b) shows that the negative vorticity has been moved closer to the flap surface and the positive vorticity (i.e. recirculation) suppressed almost entirely. The negative vorticity on the forced case confirms our previous discussion about the vortices created by the actuation and rolls down the flap surface.

One of the most interesting plots is the RMS of pressure in figure 23. This plot shows that the effect of AFC is not only affecting the wake flow, but to small extent, also the upstream flow. We notice that the RMS pressure has been increased at location b and decreased at c (see figure 4). This has not been showed by any plot previously discussed. We also notice the great suppression of P_{RMS} in the wake region (figure 24). This causes the wake structure to be less intensive and decreases the level of turbulence. A closer

look at the flap region we also conclude that the actuation is increasing the turbulence on the flap surface in order to reattach the flow. The actuation location itself is featured by increased RMS pressure. The conclusion is that the unforced case is characterized by a highly turbulent and intensive wake but the forced one by low level of turbulence in the wake, forcing makes the wake less intensive and increases the turbulence at the flap surface in order to reattach the flow.

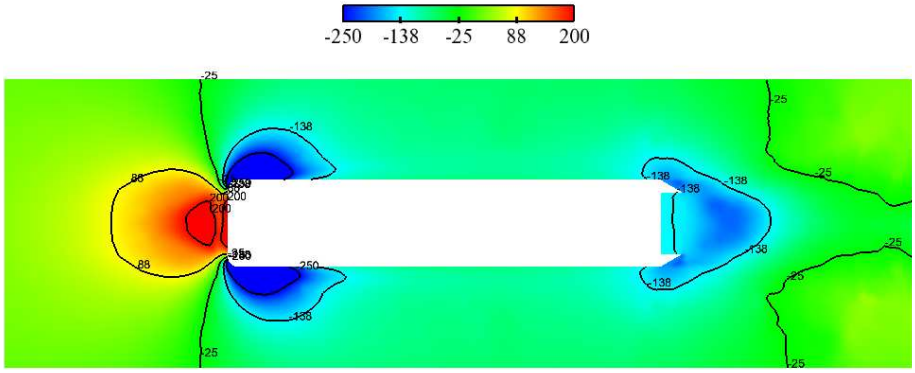

(a) AFC OFF

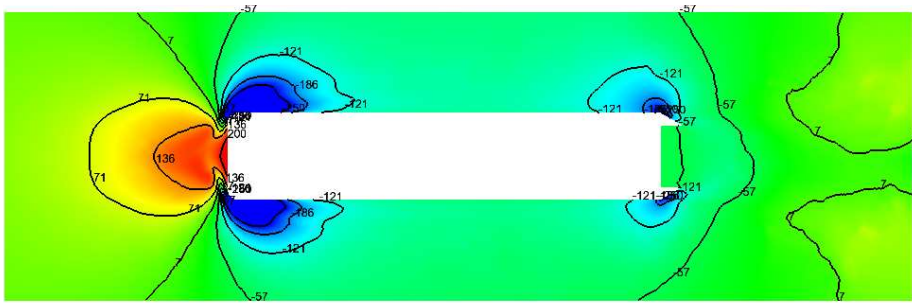

(b) AFC ON

Figure 14: Time-averaged pressure contours. Observe the large low-pressure region in (a) and how it is suppressed by AFC in (b).

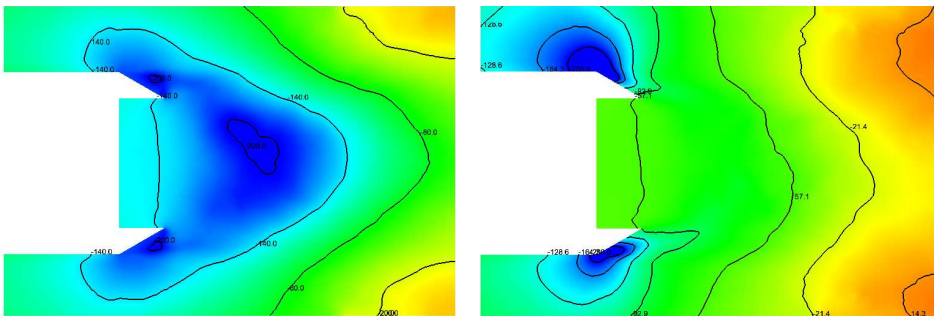

(a) AFC OFF (b) AFC ON

Figure 15: Time-averaged pressure contours, zoom of the wake.

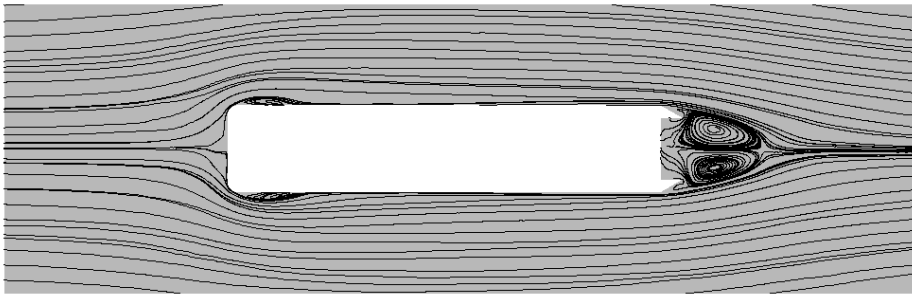

(a) AFC OFF

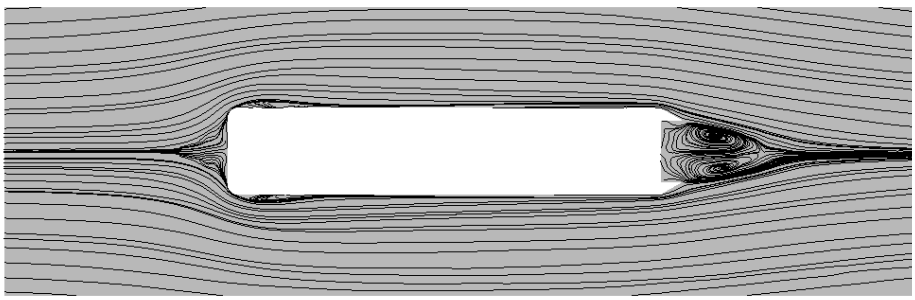

(b) AFC ON

Figure 16: Time-averaged velocity streamlines.

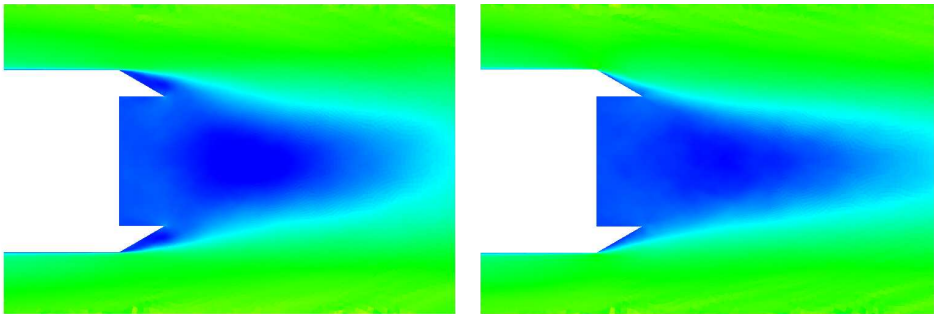

(a) AFC OFF (b) AFC ON

Figure 17: Time-averaged x-velocity contours, zoom of the wake.

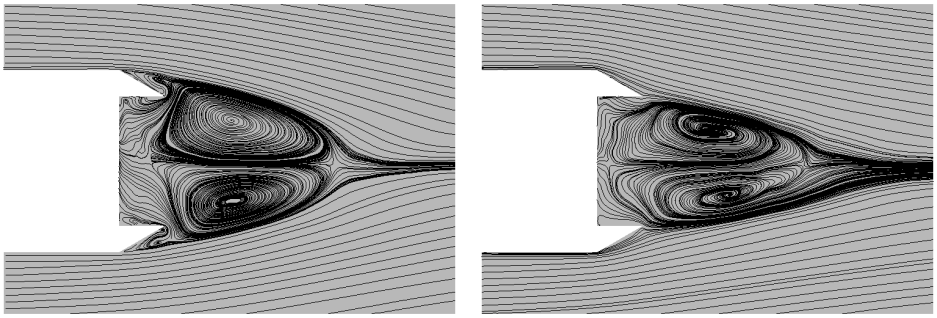

(a) AFC OFF (b) AFC ON

Figure 18: Time-averaged velocity streamlines, zoom of the wake.

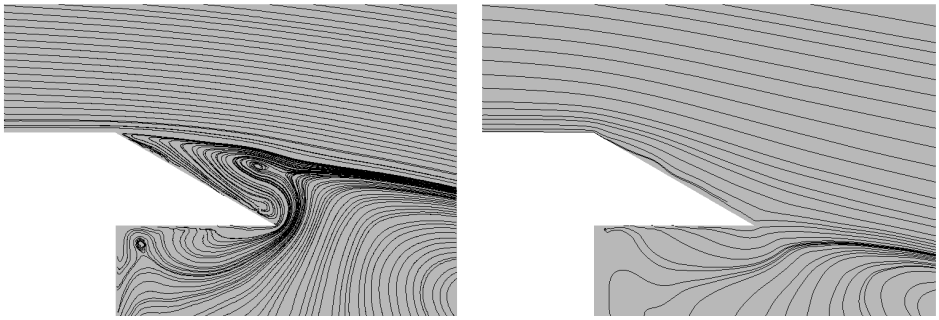

(a) AFC OFF (b) AFC ON

Figure 19: Instantaneous streamlines, zoom around flap region.

(a) AFC OFF (b) AFC ON

Figure 20: Time-averaged velocity streamlines, zoom around flap region.

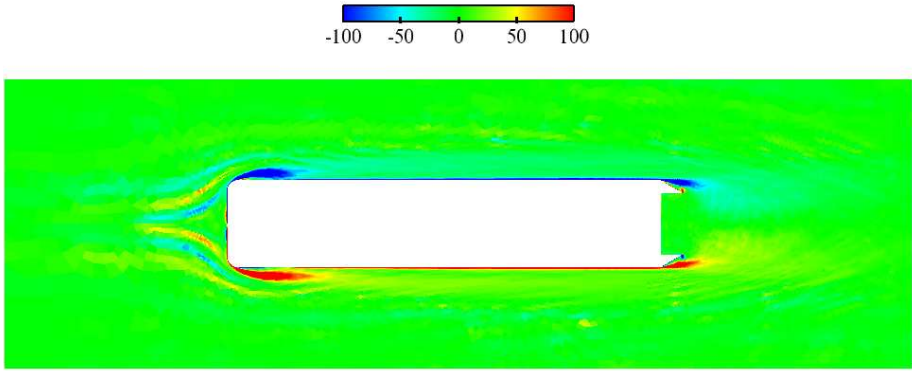

(a) AFC OFF

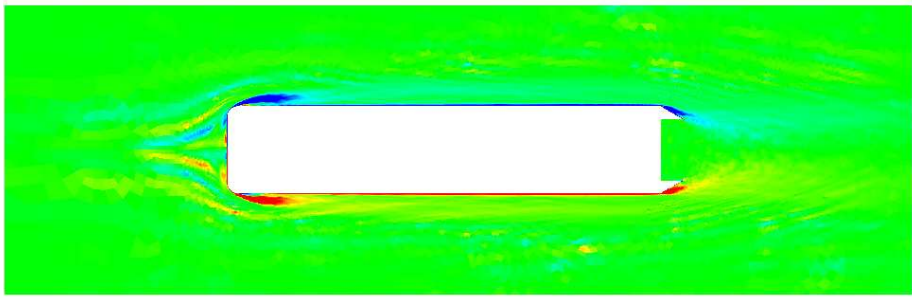

(b) AFC ON

Figure 21: Time-averaged vorticity contours.

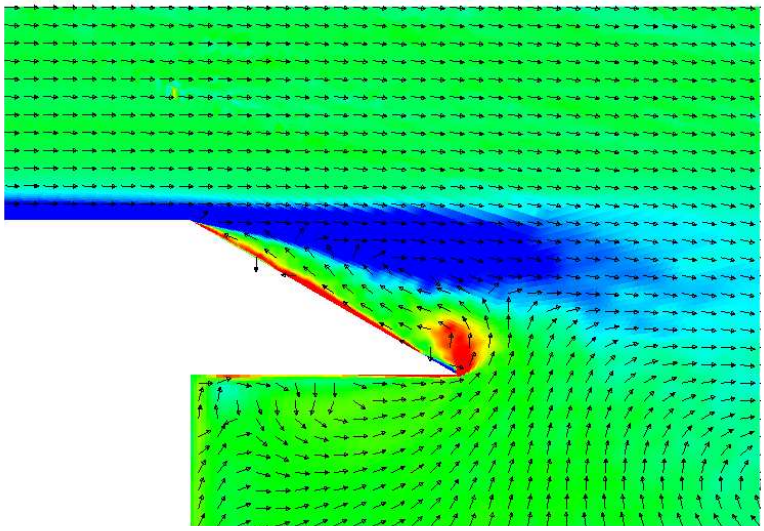

(a) AFC OFF

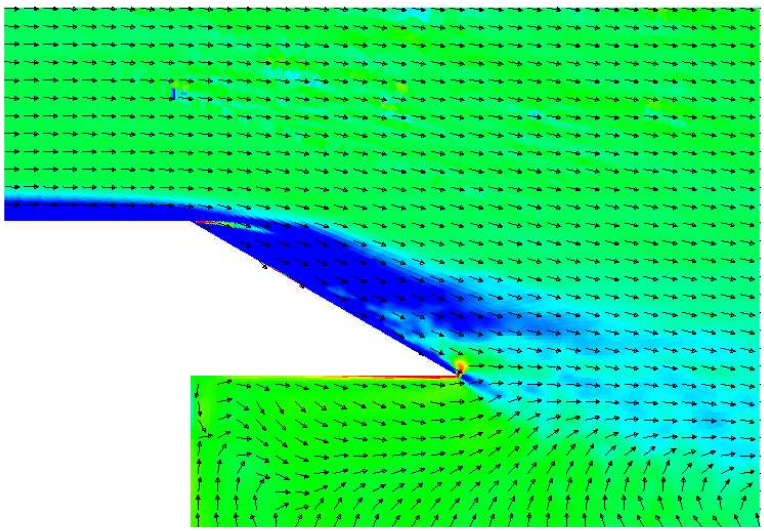

(b) AFC ON

Figure 22: Time-averaged vorticity contours and velocity vectors, zoom around flap region.

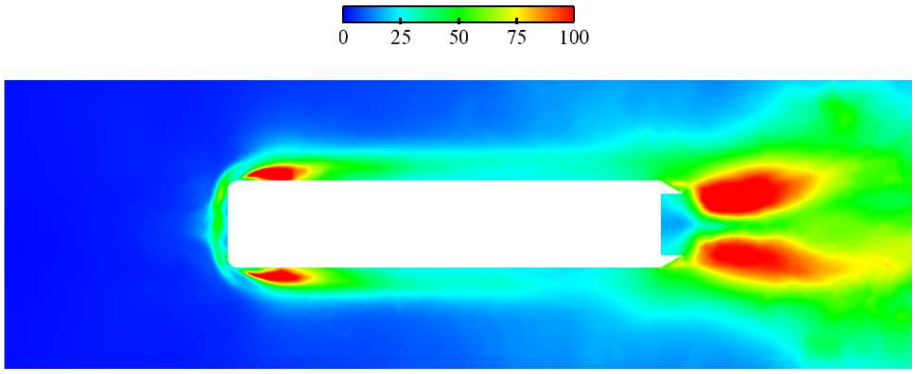

(a) AFC OFF

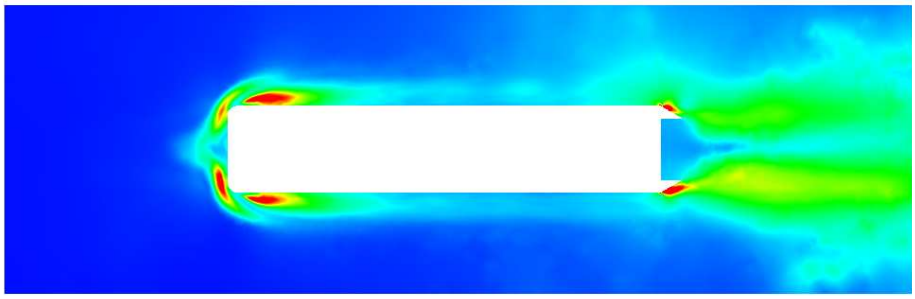

(b) AFC ON

Figure 23: RMS of pressure contours.

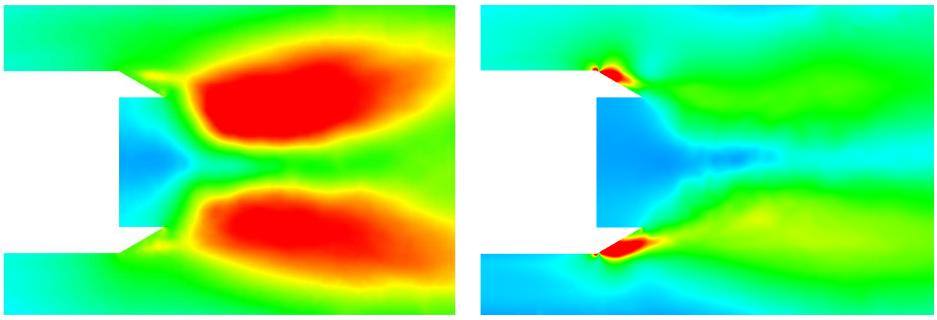

(a) AFC OFF (b) AFC ON

Figure 24: RMS of pressure contours, zoom of the wake.

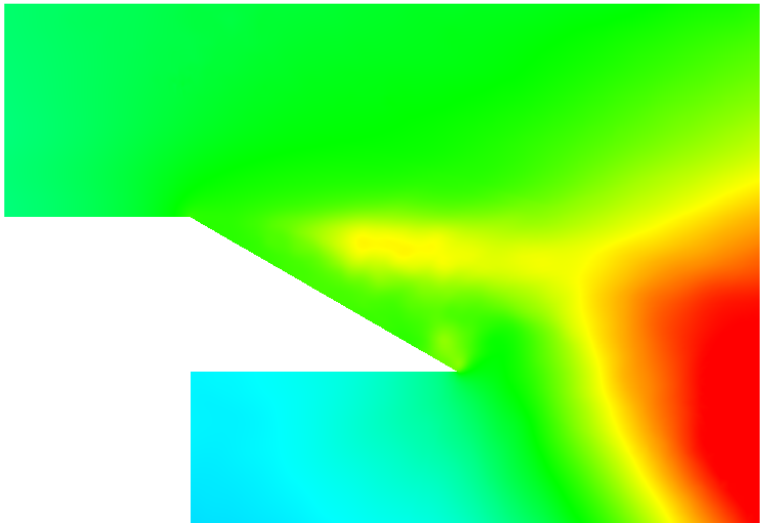

(a) AFC OFF

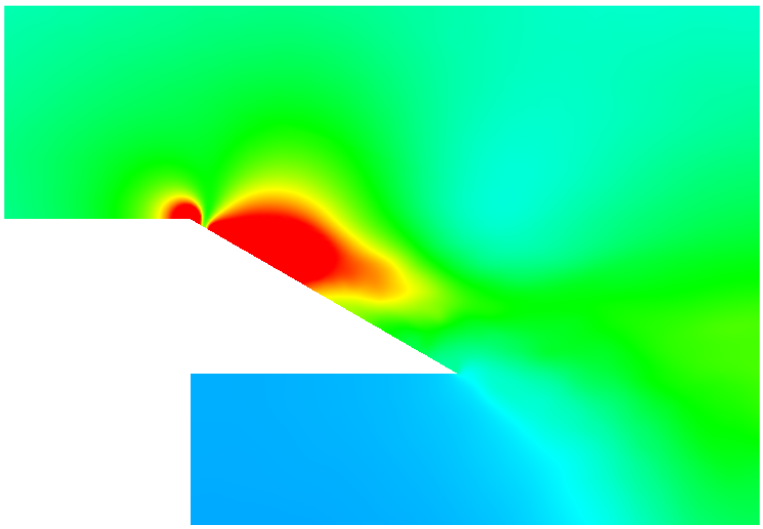

(b) AFC ON

Figure 25: RMS of pressure contours, zoom around flap region.

3.2.1 Surface pressure distribution

All location labels referred to figure 4. In order to further study the influence of AFC on the truck body, the surface pressure distribution and its RMS are plotted in figures 26 and 27. We are actually only interested in the projection of the pressure load in the x-direction because this is what contributes to the drag force. As shown in figure 26(b) the impinging location at the symmetry line is almost $C_P = 1$ as expected. The small discrepancy is mainly because the upstream domain is not large enough. C_P is then becoming negative at the curvature b and $C_{p,x}$ is exact zero on the side surface c. On the flap surface d the forced case is showing lower C_P at the slot location. However C_P increases along the flap surface and also on the rear-end of the truck at f. We notice that the main difference of the forced and unforced case is at surface f. The conclusion is that the pressure is here recovered by the AFC that minimizes the pressure difference between the front and back and thus decreases the total drag of the truck.

The surface distribution of RMS pressure is plotted in figure 27 together with the projected RMS pressure load in the x-direction. We recognize the decreased RMS in region c as discussed in section 3.2. Furthermore it is clear that the actuation is increasing the RMS at surface d but on the rear-end at f the RMS is decreased as expected. The less intensive wake in the forced case is affecting the rear truck surface.

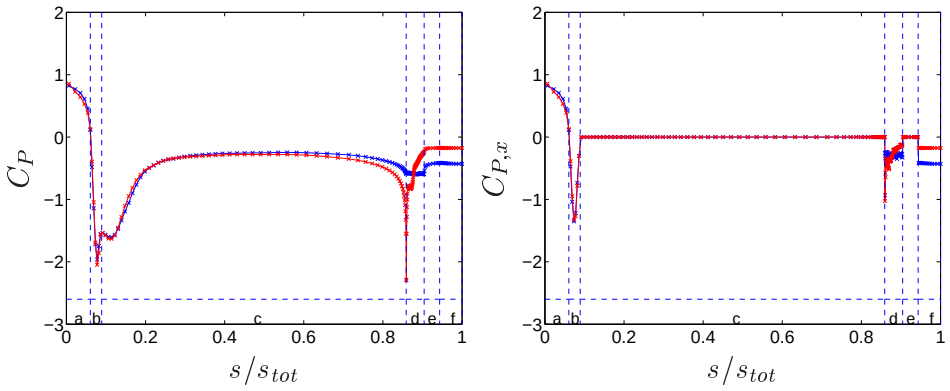

(a) Pressure coefficient.

(b) Projected pressure load in the x-direction.

Figure 26: Mean C_P and projected mean pressure load in the x-direction ($C_{P,x}$) of the upper half truck surface (symmetry). —— : AFC OFF; —— : AFC ON

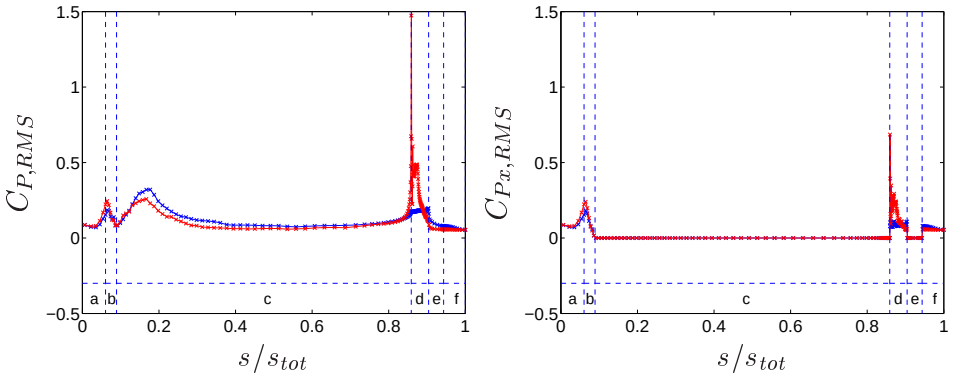

(a) RMS of Pressure.

(b) Projected RMS of pressure load in the x-direction.

Figure 27: RMS $C_{P,RMS}$ and projected RMS pressure load in the x-direction ($C_{Px,RMS}$) of the upper half truck surface (symmetry). —— : AFC OFF; —— : AFC ON

3.3 Aerodynamic forces

In figure 28(a) the drag history for both the forced and the unforced case is plotted. It is clear that the forced case shows lower drag at every instant when the flow has reach fully developed conditions. We can also conclude that the drag reduction process is done in two steps. Initially, as shown in the figure, when AFC is applied, the drag decreases a large deal (at $t = 2\ s$) before the forced flow reaches fully conditions. What probably happens is that the flow reattaches when momentum flux is added and removed to the flow via the oscillating jet. Later the forcing creates the vortices that rolls down the flap and maintain the flow reattached over the whole flap surface, keeping the drag at lower level than the unforced case.

In figure 28(b) the power spectral density of the drag signal is plotted. We notice the vortex shedding frequency in both the unforced and forced case with one difference. The peak of the forced case has been reduced compared to the unforced case. This confirms our previous discussion that the intensity of the wake is reduced by AFC. The location of these peaks are at Frequency 0.98 Hz which corresponds to Strouhal number of $St = 0.1$. This is in good agreement with measurements done on rectangular cylinders [20]. In [20] they measured the Strouhal number of rectangular cylinders of different B/H as a function of Reynolds number. For $Re = 2 \cdot 10^4$ and $B/H = 4$ the Strouhal number is $St = 0.12$. The present truck model has $B/H = 5$ at $Re = 2 \cdot 10^5$. We further notice the high peak at 10 Hz that corresponds to the actuation frequency. The intensity of the peak is high and due to this, we notice the high RMS drag of the forced case in figure

28(a).

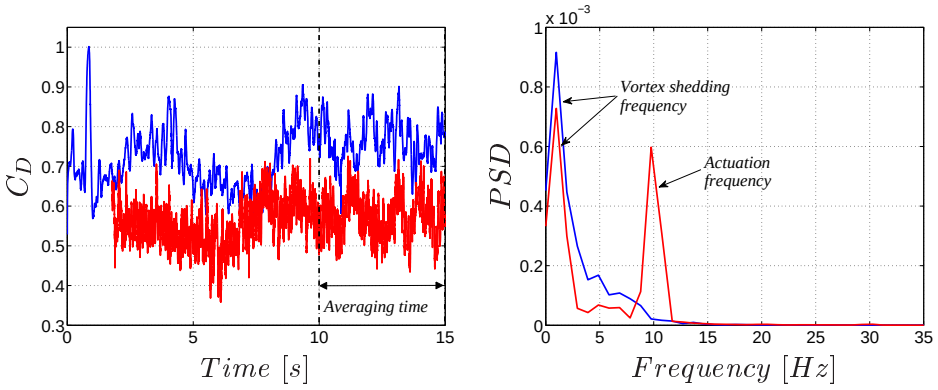

(a) Drag history

(b) Power spectral density

Figure 28: Drag history and its FFT, —— : AFC OFF; —— : AFC ON. $C_D^{AFC\ OFF} = 0.76$; $C_D^{AFC\ ON} = 0.57$. One time unit, w/U_∞, corresponds to 0.1 s.

3.4 Optimization

Five parameters were included in the optimization procedure, see table 2. The design space was chosen with knowledge gained from the large number of runs done in the first part of this work. Note that $10 < F < 25$ corresponds to $0.3 < F^+ < 0.7$ when $FL = 0.75\ m$. When $F^+ = 1$ one vortex travels with free-stream velocity to the trailing edge of the flap before the next vortex is generated. By using the inscribed central composite design as DOE with one central point, we have totally 27 cases to be run plus 9 cases without AFC. The number of unforced cases is determined by each configuration that needs to have a geometrical modification. In this case only two parameters need geometrical modification, namely FL and FA. The number of regressors is $1+2k+k(k-1)/2 = 21, (k = 5)$. The statistics of the fitted surface is found in table 3. The residuals and the studentized residuals are plotted in figure 29. One outlier was removed from the design space due to high studentized residual; also R^2_{adj} increased.

Figure 30 shows contour plots of the response surface plotted against two parameters each. The rest of the parameters were held constant. In order to search the minimum location, the gradient and all the boundaries of the design space should be checked. The minimum was found on a boundary and corresponds to the following parameters in table 4. The optimal drag value was found to be 0.28 which corresponds to 63% drag reduction compared with no AFC.

AFC parameter	Min value	Max value
FL	0.3 m	0.75 m
FA	10 deg	35 deg
SA	15 deg	35 deg
C_μ	0.1 %	1.0 %
F	10 Hz	25 Hz

Table 2: Specifications of the parameter space for optimization.

R^2	R^2_{adj}	σ^2
0.96	0.80	$4.9 \cdot 10^{-5}$

Table 3: Statistics of the fitted response surface

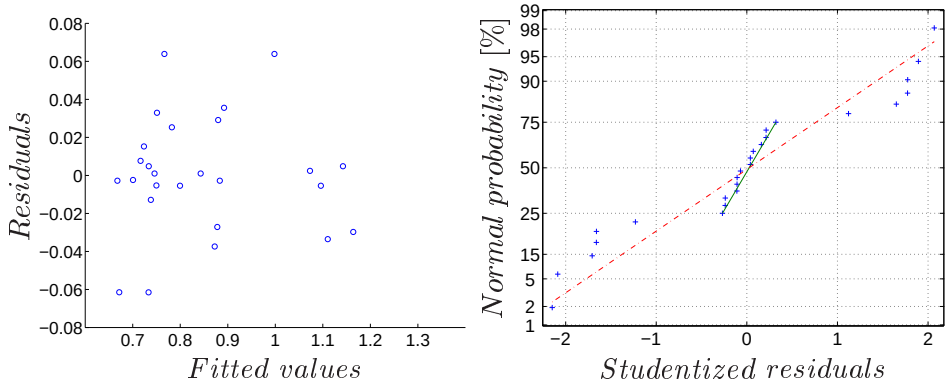

(a) Residuals

(b) Normal distribution of studentized residuals

Figure 29: Residuals of the fitted response surface.

AFC parameter	Optimal value
FL	0.6 m
FA	35 deg
SA	10 deg
C_μ	1.0 %
f	25 Hz

Table 4: Parameter values of optimal design.

By considering the plots in figure 30 it is clear that a region of feasible designs could be defined. In figure 30(b), mean drag is plotted versus FL and FA. We conclude that the length of the flap should be larger than 0.5 m and the flap angle larger than 30 deg. We also conclude that AFC can increase the drag of a truck if inappropriate values are chosen. In figure

30(d) we conclude that the influence of the slot angle is small. It is also clear from figure 30(f) that C_μ should be above 0.8 % and F large. The physical interpretation of these result is that we need a high FA and FL in order to minimize the wake size. The blowing strenth C_μ should be high in order to affect the flow and create the vortices and the frequency at 25 Hz corresponds to $F^+ = 0.6$, i.e. close to one vortex travelling along the flap surface before the next one is created.

3.5 Uncertainty issues

3.5.1 Span-wise domain size and grid dependence

In order to have consistent span-wise domain size a comparison of C_D of the unforced and forced case is done. The case specifications and mean C_D are listed in table 5 and the C_D history for the unforced case are plotted in figure 31.

Case #	Domain size	# cells	$\overline{C_D}^{AFC\ OFF}$	$\overline{C_D}^{AFC\ ON}$	$\Delta\overline{C_D}$
1	0.1 m	8	0.73	0.61	$0.11 \rightarrow 16\%$
2	0.2 m	8	0.86	–	–
3	0.2 m	16	0.96	0.55	$0.41 \rightarrow 43\%$
4	0.4 m	16	0.76	0.57	$0.19 \rightarrow 25\%$
5	0.4 m	32	0.97	0.71	$0.27 \rightarrow 27\%$
6	0.8 m	32	0.71	0.50	$0.20 \rightarrow 29\%$
7	1.0 m	40	0.72	0.54	$0.18 \rightarrow 25\%$

Table 5: Specifications of the span-wise domain sizes and corresponding mean drag. Max $\Delta z^+ \sim 130$ and mean $\Delta z^+ = 100$ for low resolution. Max $\Delta z^+ \sim 60$ and mean $\Delta z^+ = 50$ for high resolution. 80 000 cells are used in the $x - y$ plane, same as section 3.1-3.3

It is clear from the table and plots that the C_D RMS fluctuations are damped by increasing the size of the domain and decreasing the resolution, e.g. compare $dz = 0.1m$ / 8 $layers$ with $dz = 0.2m$ / 16 $layers$ and $dz = 0.2m$ / 8 $layers$ with $dz = 0.2m$ / 16 $layers$ in figure 31(a). We can also notice this tendency in figure 31(b) by comparing $dz = 0.4m$ / 16 $layers$ with $dz = 0.4m$ / 32 $layers$ and $dz = 0.4m$ / 16 $layers$ with $dz = 1.0m$ / 40 $layers$ which has the same resolution. The effect of span-wise size and resolution on the time-averaged drag seems to be the same with forcing as without.

In figure 32 the drag history for the unforced and forced case are plotted for cases 1, 3, 6 and 7. It is clear how the RMS of drag is reduced by increasing the size of the domain. The drag reduction is obvious for all cases and the RMS of drag decreases by increasing the domain size. We expect that the intensity of the forcing peak that appeared in figure 28(b) will decrease by increasing the domain size. We conclude that the choice of

domain size is of high importance in AFC simulations. When the domain size is small the flow becomes too two-dimensional and the RMS of the drag increases. Increasing the domain size, the three-dimensionality of the flow increases and the flow will be less sensitive to forcing by AFC.

3.5.2 Only blowing

An actuator was tested experimentally for the purpose of drag reduction on trucks showed less good ability to suck flow compared to its ability of blowing [19]. Therefore AFC with only blowing instead of blowing and suction was investigated. Everything was held constant and the velocity amplitude was manipulated as shown in figure 33. The maximum velocity is kept by taking half of the original velocity amplitude and shifting the signal so that no suction is done and the lowest velocity becomes zero. The new AFC velocity signal is $U_{new}(t) = 0.5A_{org} \sin \omega t + 0.5A_{org}$ and plotted in figure 33(a). The results in figure 33(b) are promising. It seems that blowing is enough to reach the desired drag reduction. We also notice that the RMS of the drag has been reduced substantially while the new drag is following the tendency of the old drag.

This result is of high importance considering the functionality of available actuators. When doing experimental work, other actuators than blowing and suction ones can be used, e.g. pulsed jet actuators.

3.5.3 Slot location dependence

There will be some problems manufacturing an actuator device for existing trailers. It is quite impossible to keep the actuators exactly at the edge connecting the rear-end of the trailer and the leading edge of the flap. For that purpose, two cases were run investigating the possibility to move the slot location $5 - 10$ cm downstream of the upstream edge of the flap. In figure 34(a) the drag history of location 2 and 3 corresponding to 5 cm and 10 cm respectively. The time-averaged drag are plotted in figure 34, where Δl is the distance between the upstream edge of the flap and flap and FL is the flap length. The original location corresponds to $\Delta l/FL = 1$.

It is clear that the slot location within 10 cm deviation from the corner of the truck will not affect the achieved drag reduction.

3.5.4 Turbulence modeling issues

The first author has supervised a bachelor thesis work [21] with the aim to check the turbulence modeling dependence on the AFC and predicted drag both on the identical fine mesh and a coarse one with wall-functions. The STAR-CCM+ software was chosen to investigate URANS and DES models compared with LES. $Spalart - Allmaras$, $k - \epsilon$ and $k - \omega$ SST were investigated together with DES $Spalart - Allmaras$ and DES $k - \omega$ SST.

The predicted mean drag is found in table 6. Velocity and RMS of pressure profiles were also investigated at different positions on the flap with and without AFC, and two of them are plotted in figure 35.

Turbulence Model	$\overline{C_D}$	$\overline{C_D}$ AFC ON	Reduction [%]
LES (present)	0.72	0.54	25%
$DES - SA$	0.76	0.62	18%
$DES - k - \omega\ SST$	0.76	0.65	14%
$Spalart - Allmaras$	0.48	0.27	45%
$k - \epsilon$	0.54	0.32	40%
$k - \omega\ SST$	0.74	0.65	13%

Table 6: Mean drag for different turbulence models, fine mesh.

Turbulence Model	$\overline{C_D}$ AFC OFF	$\overline{C_D}$ AFC ON	Reduction [%]
$DES - SA$	0.38	0.31	18%
$DES - k - \omega\ SST$	$--$	$--$	$--$
$Spalart - Allmaras$	0.44	0.39	11%
$k - \epsilon$	0.41	0.43	-4%
$k - \omega\ SST$	0.41	0.46	-11%

Table 7: Mean drag for different turbulence models, coarse mesh.

The fine mesh results in table 6 show that the both the DES models predicts the unforced case well compared to LES. $k - \epsilon$ and $Spalart - Allmaras$ fail and under-predict by approximately 30%. However $k - \omega\ SST$ shows good agreement with DES and LES. None of the DES models predict the full effect of AFC. The drag for the forced case is overpredicted by all the models that showed good prediction of the unforced case. The effect of AFC is captured by the $URANS$ models but the level of the drag value is underpredicted a great deal. The coarse mesh result show that the effect of AFC still is captured by the DES. The $URANS$ models fail. $Spalart - Allmaras$ captured a marginal effect. Considering the velocity profiles in figure 35(a) and 35(b) it is clear that all the models predicts the separation on the flap surface but none of the $URANS$ models predicted the fully attached flow at $x/W = 5.2$. The upstream and downstream edges of the flap are located at $x/w = 5.0$ and $x/w = 5.25$ respectively. The RMS of the pressure profiles are plotted in figure 35(c) and 35(d). None of the $URANS$ models predicts the profile for the unforced case whereas $DES - k - \omega\ SST$ predicts the profiles well. Both $Spalart - Allmaras$ and $k - \epsilon$ overpredicts the increased RMS at $x/w = 5.2$. The DES models is in better agreement both considering the shape of the profiles and the order of magnitude of the RMS of pressure.

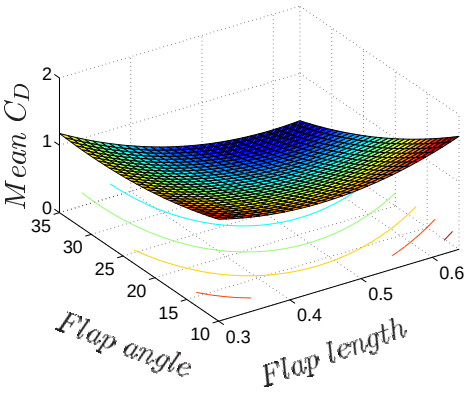

(a) 3D surface

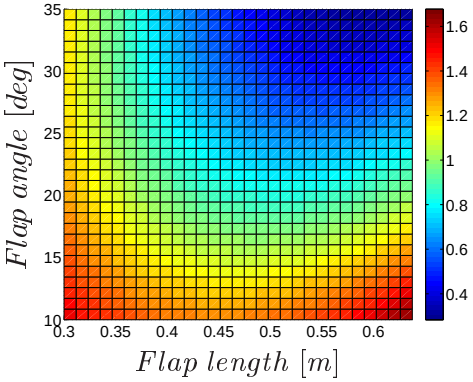

(b) Projected 2D, $SA = 10deg$, $C_\mu = 1.0$, $F = 25Hz$

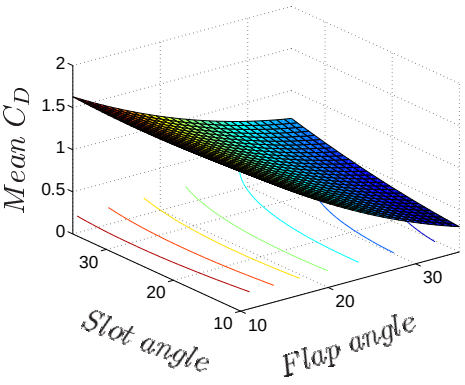

(c) 3D surface

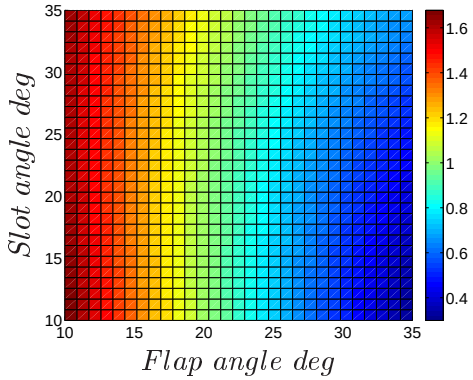

(d) Projected 2D, $FL = 0.6375\ m$, $C_\mu = 1.0$, $F = 25\ Hz$

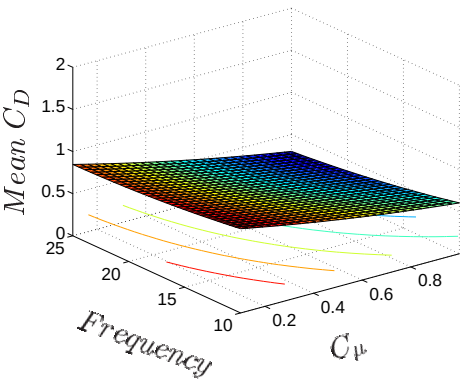

(e) 3D surface

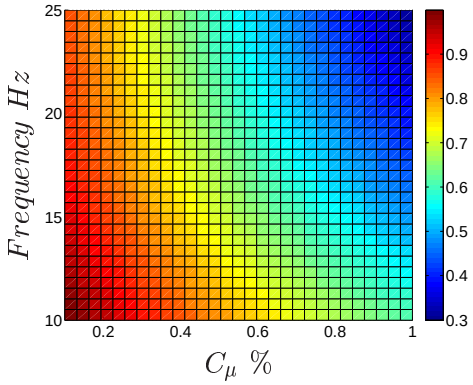

(f) $FL = 0.6375m$, $FA = 35$, $SA = 10\ deg$

Figure 30: The obtained response surface versus design parameters at optimal minimum.

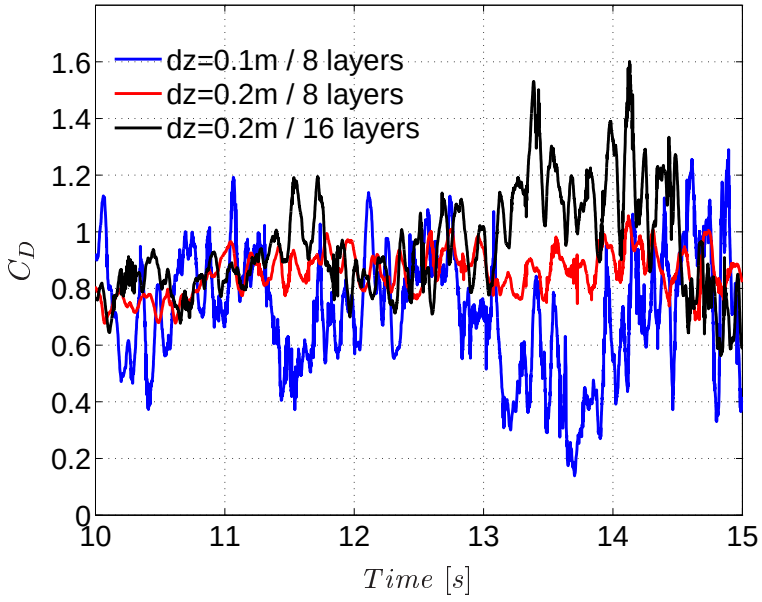

(a) Small domains

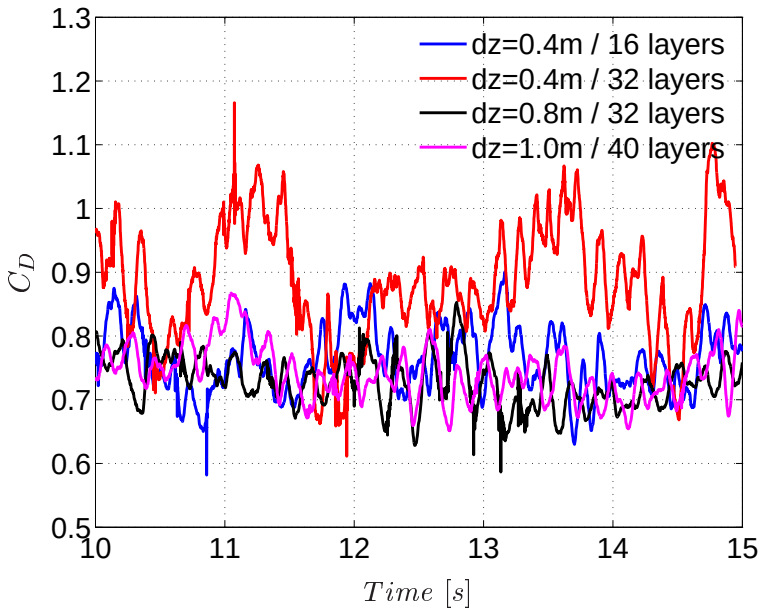

(b) Large domains

Figure 31: Drag history for different span-wise domain sizes and corresponding resolution.

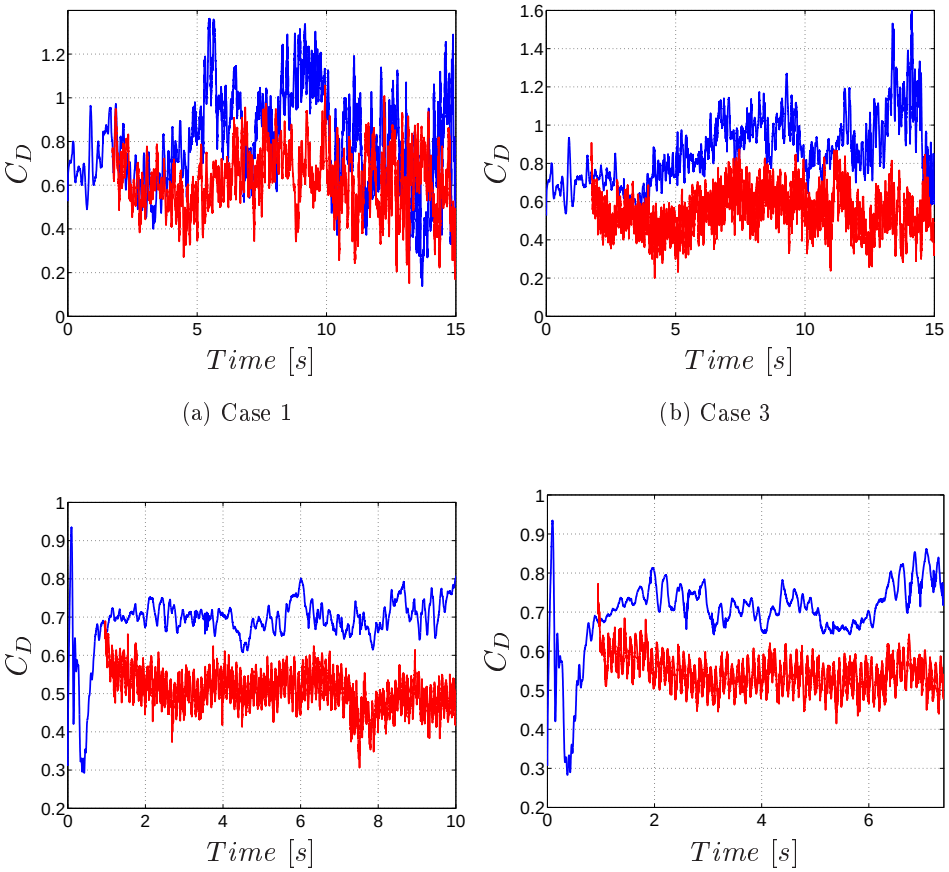

(a) Case 1

(b) Case 3

(c) Case 6

(d) Case 7

Figure 32: Drag history for different span-wise domain sizes, —— : AFC OFF; —— : AFC ON

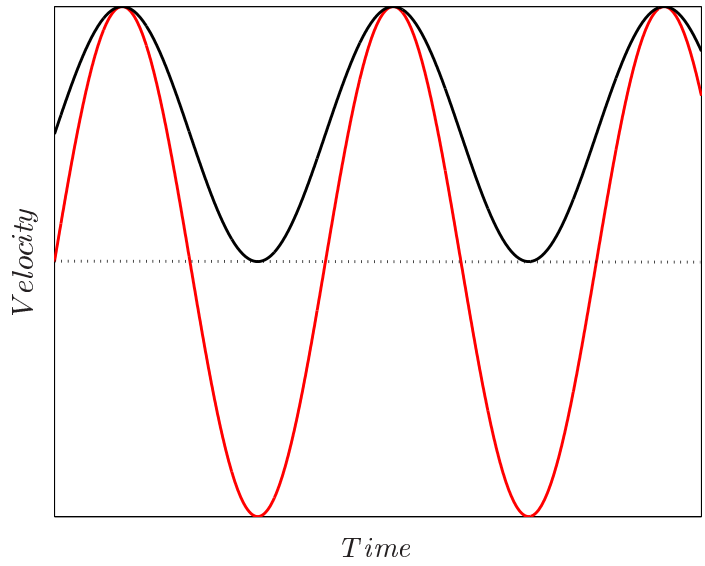

(a) Time history of AFC velocity in the slot

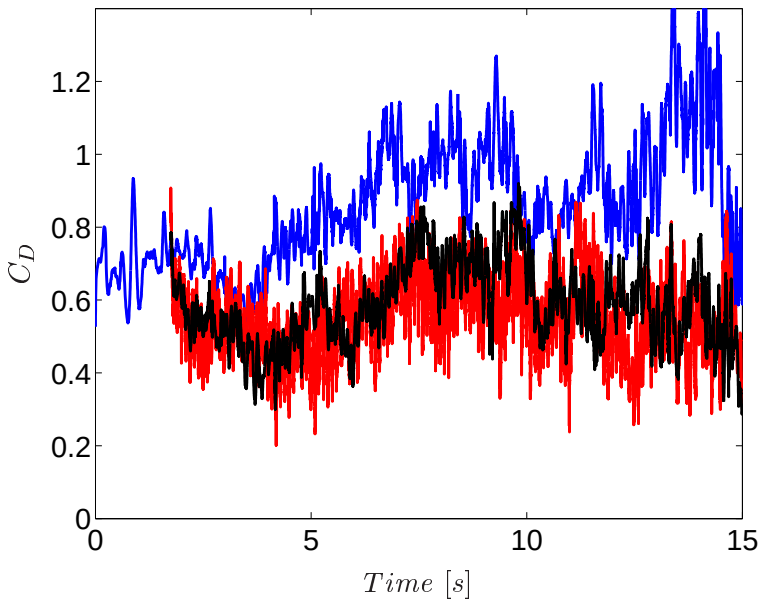

(b) Drag history

Figure 33: Drag history of unforced, forced and forced with only blowing, —— : AFC OFF; —— : AFC ON; —— : AFC ON (only blowing)

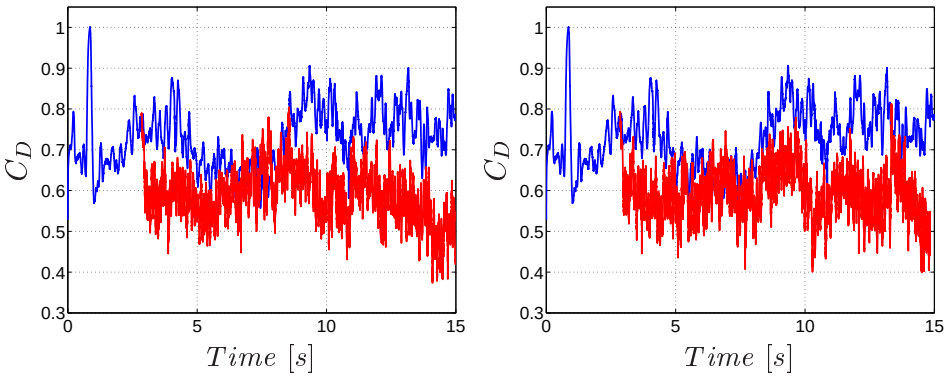

(a) Location 2

(b) Location 3

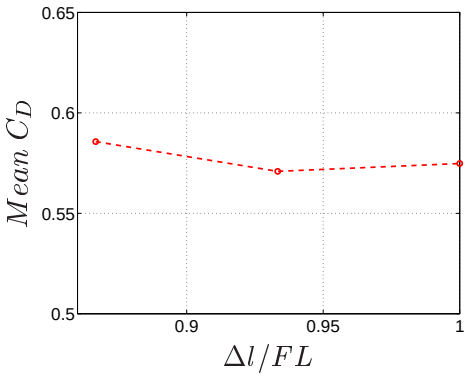

(c) Drag history

Figure 34: Drag history and time-averaged at different locations, —— : AFC OFF; —— : AFC ON

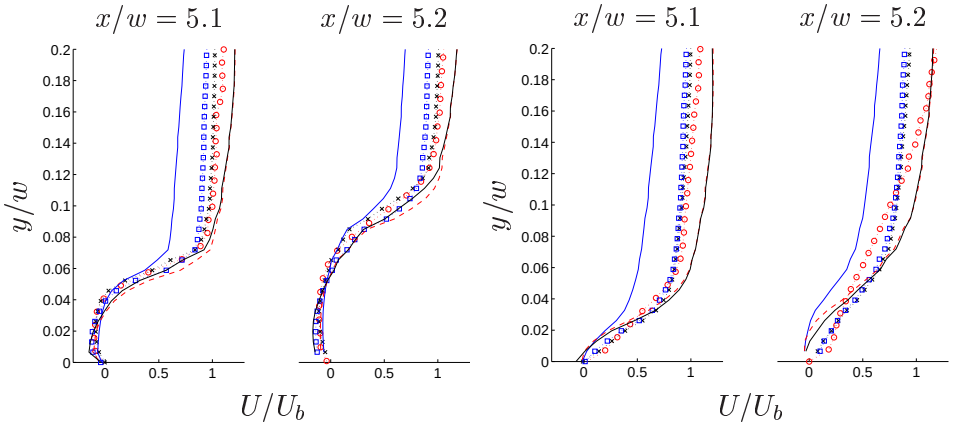

(a) AFC OFF (b) AFC ON

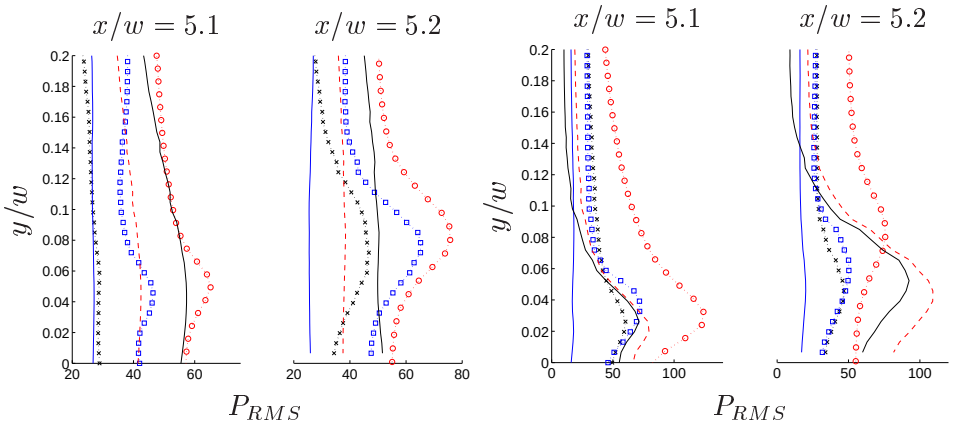

(c) AFC OFF (d) AFC ON

Figure 35: Mean velocity and RMS of pressure profiles with different turbulence models, $\cdots o \cdots$: LES; $\cdots \square \cdots$: $DES\ k-\omega\ SST$; $\cdots * \cdots$: $DES\ Spalart-Allmaras$; $- - -$: $k-\epsilon$; $\_\_\_$: $k-\omega\ SST$; $\_\_\_$: $Spalart-Allmaras$

4 Conclusions

A novel rear-end of truck-trailer is proposed, reducing the drag by 30% or more. Several hundred of large-eddy simulation cases were carried out with and without AFC and finally an optimal case is found using response surface methodology. The drag reduction is comfirmed by several flow physical analysis comparing the instantaneous and time-averaged flow field between the unforced and the forced case.

The instantaneous characteristics of the unforced case were found to typical of bluff body flows with strong global vortex-shedding and reversed flow on the flaps due to higher flap angle than the natural separation angle. The forced case has weaker vortex shedding and small vortices were observed on the flap surface, created by the actuation. These vortices are moving downstream the flap surface, creating a shear layer in the wake that prevents the interaction between the naturally created shear-layers on the upper and lower edges.

The unforced case has large time-averaged low-pressure region in the wake and on the flap surface, yielding large wake structure with high intensity and large mean drag. The flap region of the unforced case has a separated flow region whereas the actuation forced the time-averaged flow to stay attached. There is a great suppression of RMS of pressure in the wake due to AFC that decreases the level of vortex shedding in the wake and makes the wake less intensive. However the RMS of pressure was increased on the flap surface with actuation which created a strong low-pressure region at the leading edge of the flap which makes the flow to stay attached.

The low drag of the forced case is due to the increased base pressure at the rear-end of the truck, shown by the C_p analysis. The vortex-shedding frequency was in good agreement with experimental results [20]. The actuation frequency was observed in the frequency analysis of drag history which also showed that the intensity of the vortex-shedding was decreased due to AFC.

The optimization procedure using RSM defined a feasible region of the parameter values governing flap geometry and AFC variables. The flap length and angle should be larger than 0.5 m and 30 deg respectively. The slot angle has to be between $SA = 10 - 25$ deg, C_μ should be above 0.8 % and the frequency f between $10 - 25$ Hz. The optimal case was found to have drag of 0.28 which corresponds to 63% drag reduction.

By using periodic blowing as actuation instead of periodic blowing and suction, the RMS of drag were strongly reduced and the drag reduction by the blowing and suction was not affected. The slot location can be moved up to 10 cm from the corners of the truck without affecting the achieved drag reduction. The span-wise domain and mesh resolution were also investigated. The RMS of drag was decreased with larger span-wise domain size and lower mesh resolution. The flow becomes more two-dimensional

when the domain size is small and the three-dimensionality and the effect of AFC is much more clear in large domains. The achieved drag reduction is consistent with different span-wise domain sizes.

Both $DES\ k-\omega\ SST$ and $DES\ Spalart-Allmaras$ predicted the drag of the unforced case well. The effect of AFC was somewhat under-predicted. URANS models failed to predict the drag both for the forced and unforced case. $k-\omega\ SST$ was promising on the fine mesh but completely failed to predict the effect of AFC on the coarse mesh.

5 Acknowledgments

This work is supported by the **Swedish Agency of Innovation Systems (VINNOVA)**, **Volvo 3P**, **SKAB** and **CD-ADAPCO**. Financial support by SNIC (the Swedish National Infrastructure for Computing) for computer time at C3SE (Chalmers Centre for Computational Science and Engineering) is gratefully acknowledged.

References

[1] L. Hjelm and B. Bergqvist. European truck aerodynamics - a comparison between conventional and coe truck aerodynamics and a look into future trends and possibilities. In *The Aerodynamics of Heavy Vehicles II: Trucks, Buses and Trains.*

[2] M. El-Alti, P. Kjellgren, and L. Davidson. On the Download Alleviation for the XV-15 Wing by Active Flow Control Using Large-Eddy Simulation. In *ERCOFTAC Workshop: Direct and Large-Eddy Simulation 7*, Trieste, Italy, Sept 8-10 2008.

[3] P. Kjellgren, M. El-Alti, and L. Davidson. Download alleviation of a tilt-rotor wing by active flow control strategies. In *KATnet II Conference: Key Aerodynamic Technologies*, Bremen, Germany, May 12-14 2009.

[4] P. Kjellgren, N. Anderberg, and I. Wyganski. Download alleviation by periodic excitation on a typical tilt-rotor configuration - computation and experiment. In *Fluids 2000 Conference and Exhibit*, Denver, CO, June 19-22 2000.

[5] P. Kjellgren, A. Hassan, J. Sivasubramanian, L. Cullen, D. Cerchie, and I. Wyganski. Download alleviation for the XV-15: computations and experiments of flows around the wing. In *Biennial International Powered Lift Conference and Exhibit*, Williamsburg, Virginia, Nov 5-7 2002.

[6] A. Darabi and I. Wygnanski. Active management of naturally separated flow over a solid surface. part 1. the forced reattachment process. *Journal of Fluid Mechanics*, 510:105–129, 2004.

[7] M. Gad-El-Hak and Andrew Pollard. *Flow Control: Fundamentals and Practices.* Springer-Verlag Berlin Heidelberg, Germany, 1998.

[8] M. Gad-El-Hak. *Flow Control: Passive, Active and Reactive Flow Management.* Cambridge University Press, London, United Kingdom, 2000.

[9] R. Pankajakshan, Brent Mitchell, and David L. Whitfield. Full-scale simulations of drag reduction devices for class 8 trucks. In *The Aerodynamics of Heavy Vehicles II: Trucks, Buses and Trains.*

[10] J. Leuchen and K. R. Cooper. Summary of full-scale wind tunnel tests of aerodynamic drag-reducing devices for tractor-trailers. In *The Aerodynamics of Heavy Vehicles II: Trucks, Buses and Trains.*

[11] A. Seifert, O. Stalnov, D. Sperber, G. Arwatz, V. Palei, S. David, I. Dayan, and I. Fono. Large trucks drag reduction using active flow

control. In *The Aerodynamics of Heavy Vehicles II: Trucks, Buses and Trains.*

[12] L. Henning and R. King. Drag reduction by closed-loop control of a separated flow over a bluff body with a blunt trailing edge. In *44th IEEE Conference on Decision and Control and European Control Conference ECC 2005*, pages 494–499, Seville, Spain, 2005.

[13] L. Taubert and I. Wygnanski. Preliminary experiments applying active flow control to a 1/24th scale model of a semi-trailer truck. In *The Aerodynamics of Heavy Vehicles II: Trucks, Buses and Trains.*

[14] C. N. Nayeri, J. Haff, D. Greenblatt, L. Loefdahl, and C. O. Pashereit. Drag reduction on a generic tractor-trailer using active flow control in combination with solid flaps. In *The Aerodynamics of Heavy Vehicles II: Trucks, Buses and Trains.*

[15] R. J. Englar. Improved pneumatic aerodynamics for drag reduction, fuel economy, safety and stability increase for heavy vehicles. In *SAE 2005 Commercial Vehicle Engineering, Comgress and Exhibition*, SAE Paper 2005-01-3627, Chicago, Illinois, USA, 2005.

[16] A. Seifert, T. Bachar, D. Koss, M. Shepshelovich, and I. Wygnanski. Oscillatory bolwing: A tool to delay boundary-layer separation. *AIAA Journal*, 31(11):2052–2060, 1993.

[17] R. H. Myers and D. C. Montgomery. *Responce Surface Methodology: Process and Product Optimization Using Designed Experiments.* A Wiley-Interscience Publication, USA, 2002.

[18] The MathWorks Inc. MATLAB documentation, 2007.

[19] M. El-Alti, V. Chernoray, P. Kjellgren, and L. Davidson. Experimental investigation of a simple synthtic-jet actuator for active flow control purposes. Internal report, Div. of Fluid Dynamics, Dept. of Applied Mechanics, Chalmers University of Technology, Göteborg, Sweden, 2009.

[20] A. Okajima. Strouhal numbers of rectangular cylinders. *Journal of Fluid Mechanics*, 123:379–398, 1982.

[21] K. Engelbrektsson, D. Engerberg, J. Zackrisson, A. Olsson, P. Ringqvist, and M. Åslund. CFD-simulering av flödet bakom en lastbil: turbulensmodeller och aktiv strömningskontroll. Kandidatarbete 2009:03, Div. of Fluid Dynamics, Dept. of Applied Mechanics, Chalmers University of Technology, Göteborg, Sweden, 2009.